
LieTransformer: Equivariant self-attention for Lie Groups

Michael Hutchinson^{*1} Charline Le Lan^{*1} Sheheryar Zaidi^{*1}
 Emilien Dupont¹ Yee Whye Teh^{1,2} Hyunjik Kim²

Abstract

Group equivariant neural networks are used as building blocks of group invariant neural networks, which have been shown to improve generalisation performance and data efficiency through principled parameter sharing. Such works have mostly focused on group equivariant convolutions, building on the result that group equivariant linear maps are necessarily convolutions. In this work, we extend the scope of the literature to non-linear neural network modules, namely *self-attention*, that is emerging as a prominent building block of deep learning models. We propose the `LieTransformer`, an architecture composed of `LieSelfAttention` layers that are equivariant to arbitrary Lie groups and their discrete subgroups. We demonstrate the generality of our approach by showing experimental results that are competitive to baseline methods on a wide range of tasks: shape counting on point clouds, molecular property regression and modelling particle trajectories under Hamiltonian dynamics.

1. Introduction

Group equivariant neural networks are useful architectures for problems with certain symmetries, that can be described in terms of a group (in the mathematical sense). Convolutional neural networks (CNNs) are a special case that deal with translational symmetry, in that when the input to a convolutional layer is translated, the output is also translated. This property is known as *translation equivariance*, and offers a useful inductive bias for perception tasks that usually have translational symmetry. Despite the convolutional layer having far fewer parameters than a fully-connected linear layer of the same input and output dimensionality, it is sufficiently expressive to be useful for such perception tasks. This has led to the success of CNNs in multiple domains

^{*}Equal contribution, with alphabetical ordering. See [Appendix A](#) for detailed contributions. Please cite as: [Hutchinson, Le Lan, Zaidi et al. 2020]. ¹Department of Statistics, University of Oxford, UK ²DeepMind, UK. *Work in progress.*

such as computer vision (Krizhevsky et al., 2012) and audio (Graves & Jaitly, 2014).

Following on from this success, there has been a growing literature on the study of group equivariant CNNs (G-CNNs) that generalise CNNs to deal with other types of symmetries beyond translations, such as rotations and reflections. The benefit of the G-CNN is that if it learns to detect edges or patterns at a particular orientation, then it will also have learned to detect that edge or pattern at any orientation. Instead of the data augmentation approach used for vanilla CNNs, to ‘train’ the symmetry into the model, G-CNNs instead have a built in symmetry that leads to improvements in performance and data efficiency (Cohen & Welling, 2016a;b).

All works on G-CNNs deal with CNNs i.e. linear maps with shared weights composed with pointwise non-linearities, building on the result that group equivariant linear maps (with mild assumptions) are necessarily convolutions (Kondor & Trivedi, 2018; Cohen et al., 2019; Bekkers, 2020). However there has been little work on non-linear group equivariant building blocks. In this paper we extend group equivariance to self-attention (Vaswani et al., 2017), a non-trivial non-linear map, with the following motivations: (1) Self-attention has become a prominent building block of deep learning models in various data modalities, such as natural-language processing (Vaswani et al., 2017; Brown et al., 2020), computer vision (Zhang et al., 2019; Parmar et al., 2019b), reinforcement learning (Parisotto et al., 2020), and audio generation (Huang et al., 2019). (2) While convolutions are inherently translation equivariant, self-attention is permutation equivariant, hence it is a natural starting point for generalising permutation equivariance to other groups.

We thus propose `LieTransformer`, a group invariant Transformer built from equivariant `LieSelfAttention` layers. It uses a lifting based approach, that relaxes constraints on the attention module compared to approaches without lifting. Our method is applicable to Lie groups and their discrete subgroups (e.g. cyclic groups C_n and dihedral groups D_n) acting on homogeneous spaces. We consider a wide range of tasks to demonstrate the generality of our approach, namely shape counting on point clouds, molecular property regression and modelling particle trajectories under Hamiltonian dynamics.

2. Background

We begin by introducing several concepts that are necessary for the rest of the paper, namely group equivariance, equivariant maps on homogeneous input spaces, group equivariant convolutions and self-attention.

2.1. Group Equivariance

Central to our work are the concepts of group theory and representation theory. This section lays down some of the necessary definitions and notations. For a more formal overview of the topic, we refer the reader to [Esteves \(2020\)](#).

Loosely speaking, a group is a set of symmetries.

Definition 1. A **group** G is a set endowed with a single operator $\cdot : G \times G \mapsto G$ such that

1. *Associativity:* $\forall g, g', g'' \in G, (g \cdot g') \cdot g'' = g \cdot (g' \cdot g'')$
2. *Identity:* $\exists e \in G, \forall g \in G, g \cdot e = e \cdot g = g$
3. *Invertibility:* $\forall g \in G, \exists g^{-1} \in G, g \cdot g^{-1} = g^{-1} \cdot g = e$

An example of a discrete (finite) group is C_n , the set of rotational symmetries of a regular n -gon.

Note that there are n such rotations, including the identity. An example of a continuous (infinite) group is $SO(2)$, the set of all 2D rotations. C_n is a subset of $SO(2)$, hence we call C_n a **subgroup** of $SO(2)$. Note that $SO(2)$ can be parameterised by the angle of rotation $SO(2) = \{g_\theta : \theta \in [0, 2\pi)\}$. Such groups that can be continuously parameterised by real values are called **Lie groups**. Formally, a Lie group is a finite-dimensional real smooth manifold, in which group multiplication and inversion are both smooth maps. The general linear group $GL(n, \mathbb{R})$ of invertible $n \times n$ matrices is an example of a Lie group.

We can define how a group *acts* on an object using symmetry transformations as follows:

Definition 2. Let S be a set, and let $\text{Sym}(S)$ denote the set of invertible functions from S to itself. We say that a group G **acts** on S via an action $\rho : G \rightarrow \text{Sym}(S)$ when ρ is a group **homomorphism**: $\rho(g_1 g_2)(s) = (\rho(g_1) \circ \rho(g_2))(s) \forall s \in S$.

If S is a vector space V and this action is, in addition, a linear function, i.e. $\rho : G \rightarrow GL(V)$, where $GL(V)$ is the set of linear invertible functions from V to itself, then we say that ρ is a **representation** of G .

For $SO(2)$, the standard rotation matrix is an example of a representation that acts on $V = \mathbb{R}^2$:

$$\rho(g_\theta) = \begin{bmatrix} \cos \theta & -\sin \theta \\ \sin \theta & \cos \theta \end{bmatrix} \quad (1)$$

Note that this is only one of many possible representations of $SO(2)$ acting on \mathbb{R}^2 (e.g. replacing θ with $n\theta$ yields

another valid representation), and $SO(2)$ can act on spaces other than \mathbb{R}^2 e.g. \mathbb{R}^d for arbitrary $d \geq 2$.

In the context of group equivariant neural networks, V is commonly defined to be the space of scalar-valued functions on some set S , so that $V = \{f \mid f : S \rightarrow \mathbb{R}\}$. This set could be a Euclidean input space e.g. a grey-scale image can be expressed as a feature map from pixel coordinates to pixel intensities $f : \mathbb{R}^2 \rightarrow \mathbb{R}$ supported on the grid of pixel coordinates. We may express the rotation of the image as a representation of $SO(2)$ by extending the action ρ on the pixel coordinates to a representation π that acts on the space of feature maps:

$$[\pi(g_\theta)(f)](x) \triangleq f(\rho(g_\theta^{-1})x). \quad (2)$$

As a special case, we can define $V = \{f \mid f : G \rightarrow \mathbb{R}\}$ to be the space of scalar-valued functions on the group G , for which we can define a representation π acting on V via the **regular representation**:

$$[\pi(g_\theta)(f)](g_\phi) \triangleq f(g_\theta^{-1}g_\phi). \quad (3)$$

Here the action ρ is replaced by the action of the group on itself. If we wish to handle multiple channels of data, e.g. RGB images, we can stack these feature maps together, transforming in a similar manner.

Now let us define the notion of equivariance with respect to a group.

Definition 3. We say that a map $\Phi : V_1 \rightarrow V_2$ is **G -equivariant** with respect to representations ρ_1, ρ_2 of G acting on V_1, V_2 respectively if: $\Phi[\rho_1(g)f] = \rho_2(g)\Phi[f]$ for any $g \in G, f \in V_1$.

In the above example of rotating RGB images, we have $G = SO(2)$ and $\rho_1 = \rho_2 = \pi$. Hence the equivariance of Φ means that rotating an input image and then applying Φ yields the same result as first applying Φ to the original input image and then rotating the output, i.e. Φ *commutes* with the representation π .

The end goal for group equivariant neural networks is to design a neural network that obeys certain symmetries in the data. For example, we may want an image classifier to output the same classification when the input image is rotated. So in fact we want a G -invariant neural network, where the output is invariant to group actions on the input space. Note that G -invariance is a special case of G -equivariance, where ρ_2 is the *trivial representation* i.e. $\rho_2(g)$ is the identity map for any $g \in G$. Invariant maps are easy to design, by discarding information, e.g. pooling over spatial dimensions is invariant to rotations and translations. However, such maps are not expressive as they fail to extract high-level features from the data.

This is where equivariant neural networks become relevant; the standard recipe for constructing an expressive invariant

neural network is to compose multiple equivariant layers with a final invariant layer. It is a standard result that such maps are invariant (e.g. Bloem-Reddy & Teh (2019)) and a proof is given in Appendix B for completeness.

2.2. Equivariant Maps on Homogeneous Input Spaces

In this section we introduce the framework for G -equivariant maps, and provide group equivariant convolutions as an example. Suppose we have data in the form of a set of input pairs $(x_i, \mathbf{f}_i)_{i=1}^n$ where $x_i \in \mathcal{X}$ are spatial coordinates and $\mathbf{f}_i \in \mathcal{F}$ are feature values. In practice $\mathcal{X} = \mathbb{R}^{d_x}$, $\mathcal{F} = \mathbb{R}^{d_f}$. We assume that a group G acts on the x -space \mathcal{X} via action ρ , and that the action is **transitive** (also referred to as \mathcal{X} is **homogeneous**). This means that all elements of \mathcal{X} are connected by the action: $\forall x, x' \in \mathcal{X}, \exists g \in G : \rho(g)x = x'$. Let us write gx instead of $\rho(g)x$ to reduce clutter.

Now say we choose some origin $x_0 \in \mathcal{X}$. Then each $x \in \mathcal{X}$ corresponds to the set of group elements that map x_0 to x : $\{g \in G \mid gx_0 = x\}$. This set can be defined in terms of the origin's **stabiliser** $H \triangleq \{g \in G \mid gx_0 = x_0\}$, as a (left) **coset** $gH \triangleq \{gh \mid h \in H\}$ where g is any element of $\{g \in G \mid gx_0 = x\}$ (the left coset does not depend on the choice of the element). This correspondence between x and gH is described mathematically as an isomorphism between \mathcal{X} and $G/H \triangleq \{gH \mid g \in G\}$, the set of cosets of H . So for every point $x \in \mathcal{X}$, we can choose a **representative** element $s(x) \in G$ among the elements in the coset that corresponds to x under the isomorphism, i.e. x corresponds to the coset $s(x)H$. Note that the coset $s(x_i)H$ does not depend on the choice of s , but only on the isomorphism between \mathcal{X} and G/H .

For example, when the group of 2D translations $T(2)$ acts on \mathbb{R}^2 , the stabiliser of the origin x_0 is $H = \{e\}$, a singleton identity element. Hence the only possible choice for $s(x)$ is t_x , the group element describing the translation from the origin x_0 to x . On the other hand $SO(2)$, the group of 2D rotations centered at the origin, does *not* act transitively on \mathbb{R}^2 because points that have different distances to the origin cannot be mapped onto each other via such a rotation. However the group of 2D translations and rotations $SE(2) \triangleq T(2) \times SO(2)$ acts transitively on \mathbb{R}^2 , with stabiliser $H = SO(2)$, and indeed we have $\mathbb{R}^2 \simeq G/H = SE(2)/SO(2) = T(2)$. A canonical choice for $s(x)$ is t_x , but other elements of the coset $t_x H$ are also valid.

The set of data pairs $(x_i, \mathbf{f}_i)_{i=1}^n$ can be described as a feature map $f_{\mathcal{X}} : x_i \mapsto \mathbf{f}_i$, a function from $\mathcal{X} \simeq G/H$ to \mathbb{R}^{d_f} , that can be mapped to a function from G to \mathbb{R}^{d_f} via a **lifting** layer described in Section 3.1. Let \mathcal{I}_U denote the space of such unconstrained functions from G to \mathbb{R}^{d_f} . Subsequently, we may define the group equivariant maps as functions from \mathcal{I}_U to itself.

The **group equivariant convolution** (Cohen & Welling, 2016a; Cohen et al., 2018; Finzi et al., 2020; Romero et al., 2020) is an example of such a group equivariant map that has been studied extensively. Convolutions are by definition translation equivariant: translating the input image then passing it through a convolution yields the same output as passing the original image through a convolution then translating it. Hence they are a good starting point for constructing group equivariant maps for groups that contain translations. Specifically, the group equivariant convolution $\Psi : \mathcal{I}_U \rightarrow \mathcal{I}_U$ is defined as:

$$[\Psi f](g) \triangleq \int_G \psi(g'^{-1}g)f(g')dg' \quad (4)$$

where $\psi : G \rightarrow \mathbb{R}$ is the convolutional filter and the integral is defined with respect to the left Haar measure of G . Note that for discrete groups the integral amounts to a sum over the group. Hence the integral can be computed exactly for discrete groups (Cohen & Welling, 2016a), and for Lie groups it can be approximated using Fast Fourier Transforms (Cohen et al., 2018) or Monte Carlo (MC) estimation (Finzi et al., 2020).

Given the regular representation π of G acting on \mathcal{I}_U as

$$[\pi(u)f](g) \triangleq f(u^{-1}g), \quad (5)$$

we can easily verify that Ψ is equivariant with respect to π (c.f. Appendix B).

2.3. Self-attention

Self-attention (Vaswani et al., 2017) is a mapping from an input set of N vectors $\{x_1, \dots, x_N\}$, where $x_i \in \mathbb{R}^D$, to an output set of N vectors in \mathbb{R}^D . Let us represent the inputs as a matrix $X \in \mathbb{R}^{N \times D}$ such that the i th row X_i is x_i . **Multihed self-attention** (MSA) consists of M **heads** where M is chosen to divide D . The output of each head is a set of N vectors of dimension D/M , where each vector is obtained by taking a weighted average of the input vectors $\{x_1, \dots, x_N\}$ with weights given by a weight matrix W , followed by a linear map $W^V \in \mathbb{R}^{D \times D/M}$. Using m to index the head ($m = 1, \dots, M$), the output of the m th head can be written as:

$$W \triangleq \text{softmax}(XW^{Q,m}(XW^{K,m})^\top) \in \mathbb{R}^{N \times N}$$

$$f^m(X) \triangleq WXW^{V,m} \in \mathbb{R}^{N \times D/M}$$

where $W^{Q,m}, W^{K,m}, W^{V,m} \in \mathbb{R}^{D \times D/M}$ are learnable parameters, and the softmax normalisation is performed on each row of the matrix $XW^{Q,m}(XW^{K,m})^\top \in \mathbb{R}^{N \times N}$. Finally, the outputs of all heads are concatenated into a $N \times D$ matrix and then right multiplied by $W^O \in \mathbb{R}^{D \times D}$. Hence MSA is defined by:

$$MSA(X) \triangleq [f^1(X), \dots, f^M(X)]W^O \in \mathbb{R}^{N \times D}. \quad (6)$$

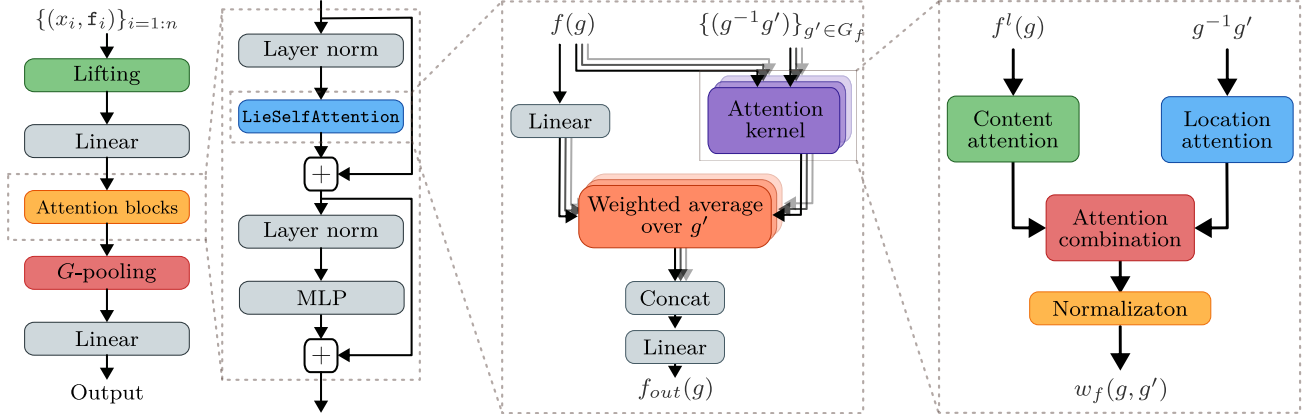


Figure 1. Architecture of the LieTransformer.

Note $XW^Q(XW^K)^\top$ is the Gram matrix for the dot-product kernel, and softmax normalisation is a particular choice of normalisation. Hence MSA can be generalised to other choices of kernels and normalisation that are equally valid (Wang et al., 2018; Tsai et al., 2019).

3. LieTransformer

We first outline the problem setting before describing our model, the LieTransformer. We tackle the problem of regression/classification for predicting a scalar/vector-valued target y given a set of input pairs $(x_i, \mathbf{f}_i)_{i=1}^n$ where $x_i \in \mathbb{R}^{d_x}$ are spatial locations and $\mathbf{f}_i \in \mathbb{R}^{d_f}$ are feature values at the spatial location. Hence the training data of size N is a set of tuples $((x_i, \mathbf{f}_i)_{i=1}^{n_j}, y_j)_{j=1}^N$. In some tasks such as point cloud classification, the feature values \mathbf{f}_i may not be given. In this case the \mathbf{f}_i can set to be a fixed constant or a function of $(x_i)_{i=1}^n$.

LieTransformer is composed of a **lifting** layer followed by residual blocks of LieSelfAttention layers, LayerNorm and pointwise MLPs, all of which are equivariant with respect to the regular representation, followed by a final invariant G-pooling layer (c.f. Appendix E for more details on these layers). We summarise the architecture in Figure 1 and provide details of its key components below. We provide all proofs of equivariance in Appendix B.

3.1. Lifting

Recall the following observations from Section 2.2:

- A set of input pairs $(x_i, \mathbf{f}_i)_{i=1}^n$ can be described as a feature map $f_{\mathcal{X}} : x_i \mapsto \mathbf{f}_i$ supported on the set $\{x_1, \dots, x_n\}$.
- For G acting on a homogeneous space \mathcal{X} , there exists an isomorphism $\mathcal{X} \simeq G/H = \{gH \mid g \in G\}$ where each x_i corresponds to the coset $s(x_i)H$ where $s(x_i)$

is a representative element of the coset.

- The coset $s(x_i)H$ does not depend on the choice of s , but only on the isomorphism between \mathcal{X} and G/H .

The **lifting** \mathcal{L} maps $f_{\mathcal{X}}$ (supported on $\bigcup_{i=1}^n \{x_i\} \subset \mathcal{X}$) to $\mathcal{L}[f_{\mathcal{X}}]$ (supported on $\bigcup_{i=1}^n s(x_i)H \subset G$) such that:

$$\mathcal{L}[f_{\mathcal{X}}](g) \triangleq \mathbf{f}_i \text{ for } g \in s(x_i)H. \quad (7)$$

This can be thought of as extending the domain of $f_{\mathcal{X}}$ from \mathcal{X} to G , while preserving the feature values \mathbf{f}_i . See Figure 2 for a visualisation.

As in Equation 2, we define the representation π on $f_{\mathcal{X}}$ as:

$$[\pi(u)f_{\mathcal{X}}](x) = f_{\mathcal{X}}(u^{-1}x) \quad (8)$$

where $u \in G$. Note $f_{\mathcal{X}}(u^{-1}x) = \mathbf{f}_i$ for $x = ux_i$, hence the action simply corresponds to mapping (x_i, \mathbf{f}_i) to (ux_i, \mathbf{f}_i) .

As in Equation 3, we may define the representation π on $\mathcal{L}[f_{\mathcal{X}}]$ as:

$$[\pi(u)\mathcal{L}[f_{\mathcal{X}}]](g) = \mathcal{L}[f_{\mathcal{X}}](u^{-1}g) \quad (9)$$

The role of this lifting layer is to move our feature maps $f_{\mathcal{X}}$, lying in the space of functions on \mathcal{X} , to the space of functions on G . We need to ensure that this is done while preserving equivariance, which is why we need the space to be homogeneous with respect to the action of G on \mathcal{X} .

Proposition 1. *The lifting layer \mathcal{L} is equivariant with respect to the representation π .*

3.2. LieSelfAttention

Let $f \triangleq \mathcal{L}[f_{\mathcal{X}}]$, hence f is defined on the set $G_f = \bigcup_{i=1}^n s(x_i)H$. We define the LieSelfAttention layer in Algorithm 1, where self-attention is defined across the

Algorithm 1 LieSelfAttention

Input: $\{f(g), g\}_{g \in G_f}$
for $g \in G_f$
 for $g' \in G_f$ (or $\text{nbhd}_\eta(g)$)
 ▷ Compute content/location attention
 $k_c(f(g), f(g')), k_l(g^{-1}g')$
 ▷ Compute unnormalised weights
 $\alpha_f(g, g') = F(k_c(f(g), f(g')), k_l(g^{-1}g'))$
 ▷ Compute normalised weights and output
 $\{w_f(g, g')\}_{g' \in G_f} = \text{norm}\{\alpha_f(g, g')\}_{g' \in G_f}$
 $f_{out}(g) = \int_{G_f} w_f(g, g') W^V f(g') dg'$

Output: $\{f_{out}(g)\}_{g \in G_f}$

elements of G_f . We first describe the method for finite G_f , and then generalise to infinite G_f at the end of the section.

There are various choices for functions k_c that represents content-based attention, k_l that represents location-based attention, F that determines how to combine the two to form unnormalised weights, and the choice of normalisation of weights. We explore the following non-exhaustive list of choices:

Content-based attention $k_c(f(g), f(g'))$:

1. Dot-product: $\frac{1}{\sqrt{d_v}} (W^Q f(g))^\top W^K f(g') \in \mathbb{R}$
 for $W^Q, W^K \in \mathbb{R}^{d_v \times d_v}$
2. Concat: $\text{Concat}[W^Q f(g), W^K f(g')] \in \mathbb{R}^{2d_v}$
3. Linear-Concat-linear:
 $W \text{Concat}[W^Q f(g), W^K f(g')] \in \mathbb{R}^{d_s}$
 for $W \in \mathbb{R}^{d_s \times 2d_v}$.

Location-based attention $k_l(g^{-1}g')$ for Lie groups G :

1. Plain: $\nu[\log(g^{-1}g')]$
2. MLP: $\text{MLP}(\nu[\log(g^{-1}g')])$

where $\log : G \rightarrow \mathfrak{g}$ is the log map from G to its Lie algebra \mathfrak{g} , and $\nu : \mathfrak{g} \rightarrow \mathbb{R}^d$ is the isomorphism that extracts the free parameters from the output of the log map (Finzi et al., 2020). We can use the same log map for discrete subgroups of Lie groups (e.g. $C_n \leq SO(2), D_n \leq O(2)$). See Appendix C for an introduction to the Lie algebra and the exact form of $\nu \circ \log(g)$ for common Lie groups.

Combining content and location attention $\alpha_f(g, g')$:

1. Additive: $k_c(f(g), f(g')) + k_l(g^{-1}g')$
2. MLP: $\text{MLP}[\text{Concat}[k_c(f(g), f(g')), k_l(g^{-1}g')]]$

3. Multiplicative: $k_c(f(g), f(g')) \cdot k_l(g^{-1}g')$

Note that the MLP case is a strict generalisation of the additive combination, and for this option k_c and k_l need not be scalars.

Normalisation of weights $\{w_f(g, g')\}_{g' \in G_f}$:

1. Softmax: $\text{softmax}(\{\alpha_f(g, g')\}_{g' \in G_f})$
2. Constant: $\{\frac{1}{|G_f|} \alpha_f(g, g')\}_{g' \in G_f}$

Any combination of choices leads to equivariant LieSelfAttention:

Proposition 2. *LieSelfAttention is equivariant with respect to the regular representation π .*

Multihead equivariant self-attention is a simple extension of the above single-head case. Let M be the number of heads, assuming it divides d_v , with m indexing the head. Then the output of each head is:

$$V^m(g) = \int_{G_f} w_f(g, g') W^{V,m} f(g') dg' \in \mathbb{R}^{d_v/M} \quad (10)$$

The only difference is that $W^{Q,m}, W^{K,m}, W^{V,m} \in \mathbb{R}^{d_v/M \times d_v}$. The multihead self-attention combines the heads using $W^O \in \mathbb{R}^{d_v \times d_v}$, to output:

$$f_{out}(g) = W^O \begin{bmatrix} V^1(g) \\ \vdots \\ V^M(g) \end{bmatrix} \quad (11)$$

Generalisation to infinite G_f Note that for Lie Groups, G_f is usually infinite (it need not be if H is discrete e.g. for $T(n)$ acting on \mathbb{R}^n , we have $H = \{e\}$ hence G_f is finite). To deal with the infinite case we resort to Monte Carlo (MC) estimation to approximate the above integral, following the approach of Finzi et al. (2020):

1. Replace $G_f \triangleq \cup_{i=1}^n s(x_i)H$ with a finite subset $\hat{G}_f \triangleq \cup_{i=1}^n s(x_i)\hat{H}$ where \hat{H} is a finite subset of H sampled uniformly.
2. (Optional, for computational efficiency) Further replace \hat{G}_f with uniform samples from the neighbourhood $\text{nbhd}_\eta(g) \triangleq \{g' \in \hat{G}_f : d(g, g') \leq \eta\}$ for some threshold η where distance is measured by the log map $d(g, g') = \|\nu[\log(g^{-1}g')]\|$.

See Figure 2 for a visualisation. Due to MC estimation we now have equivariance in expectation as Finzi et al. (2020). For sampling within the neighbourhood, we can show that the resulting LieSelfAttention is still equivariant in expectation given that the distance is a function of $g^{-1}g'$ (c.f. Appendix B).

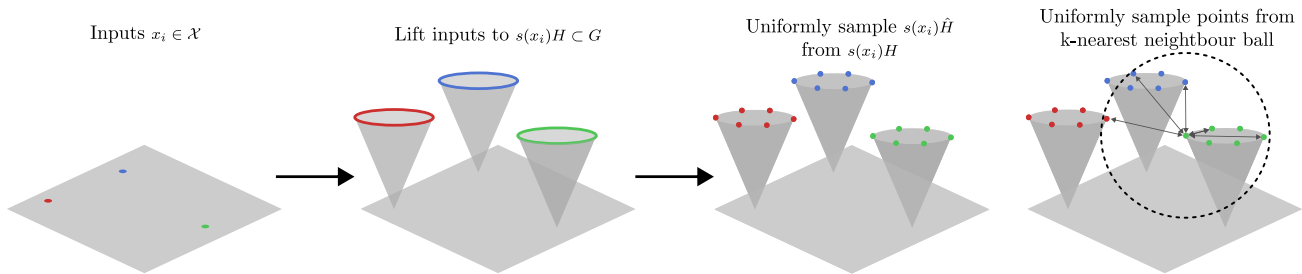


Figure 2. Visualisation of lifting, sampling \hat{H} , and subsampling in the local neighbourhood for $SE(2)$ acting on \mathbb{R}^2 . Self-attention is performed on this subsampled neighbourhood.

4. Related Work

Equivariant maps with/without lifting Equivariant neural networks can be broadly categorised by whether the input spatial data is *lifted* onto the space of functions on group G or not. Without lifting, the equivariant map is defined between the space of functions/features on the homogeneous input space X , with equivariance imposing a constraint on the parameterisation of the convolutional kernel or attention module (Cohen & Welling, 2016b; Worrall et al., 2017; Thomas et al., 2018; Kondor et al., 2018; Weiler et al., 2018b;a; Weiler & Cesa, 2019; Esteves et al., 2020; Fuchs et al., 2020). In the case of convolutions, the kernel is expressed using a basis of equivariant functions such as circular or spherical harmonics. However with lifting, the equivariant map is defined between the space of functions/features on G , and aforementioned constraints on the convolutional kernel or attention module are relaxed at the cost of an increased dimensionality of the input to the neural network (Cohen & Welling, 2016a; Cohen et al., 2018; Esteves et al., 2018; Finzi et al., 2020; Bekkers, 2020; Romero et al., 2020; Hooeboom et al., 2018). Our method also uses lifting to define equivariant self-attention.

Equivariant self-attention Most of the above works use equivariant convolutions as the core building block of their equivariant module, drawing from the result that bounded linear operators are group equivariant if and only if they are convolutions (Kondor & Trivedi, 2018; Cohen et al., 2019; Bekkers, 2020). Such convolutions are used with pointwise non-linearities (more precisely non-linearities applied independently to the features at each spatial location/group element) to form expressive equivariant maps (examples of non-linearities are given in Weiler & Cesa (2019)). Exceptions to this are Romero et al. (2020) and Fuchs et al. (2020) that explore equivariant attentive convolutions, reweighing convolutional kernels with attention weights. This gives non-linear equivariant maps with non-linear interactions across spatial locations/group elements. Instead, our work removes convolutions and investigates the use of equivariant self-attention only, inspired by works that use stand-alone self-attention on images to achieve competitive performance to

convolutions (Parmar et al., 2019a; Dosovitskiy et al., 2020). Furthermore, Romero et al. (2020) focus on image applications (hence scalability) and discrete groups (p4, p4m), and Fuchs et al. (2020) focus on point cloud applications and the $SE(3)$ group with irreducible representations. Instead we use regular representations, and attempt to give a general method for Lie groups acting on homogeneous spaces, with a wide range of applications from dealing with point cloud data to modelling Hamiltonian dynamics of particles. This is very much in the spirit of Finzi et al. (2020), except for self-attention instead of convolutions. In concurrent work, Romero & Cordonnier (2020) describe group equivariant self-attention also using lifting and regular representations. Their analogue of location-based attention are group invariant positional encodings. The main difference between the two works is that Romero & Cordonnier (2020) specify methodology for discrete groups applied to image classification only, whereas our method provides a general formula for (unimodular) Lie groups and their discrete subgroups for the aforementioned applications.

5. Experiments

We consider three different tasks that have certain symmetries, highlighting the benefits of the `LieTransformer`: (1) Counting shapes in 2D point cloud of constellations (2) Molecular property regression and (3) Modelling particle trajectories under Hamiltonian dynamics.

5.1. Counting Shapes in 2D Point Clouds

We first consider the toy, synthetic task of counting shapes in a 2D point cloud $\{x_1, x_2, \dots, x_K\}$ of constellations (Kosiorek et al., 2019). Each example consists of K points on the plane that form the vertices of multiple patterns. There are four types of patterns: triangles, squares, pentagons and the ‘L’ shape, with varying sizes, orientation, and number of instances per pattern (see Figure 3a). The task is to classify the number of instances of each pattern, hence is invariant to rotations and translations in the plane ($SE(2)$). The x_i are set to be a vector of pairwise distances to every other

Train & test config	Fixed train & test	Fixed train & augmented test		Augmented train & test		
	$D_{\text{train}}/D_{\text{test}}$	$D_{\text{train}}/D_{\text{test}}^{T2}$	$D_{\text{train}}/D_{\text{test}}^{SE2}$	$D_{\text{train}}^{T2}/D_{\text{test}}^{T2}$	$D_{\text{train}}^{T2}/D_{\text{test}}^{SE2}$	$D_{\text{train}}^{SE2}/D_{\text{test}}^{SE2}$
SetTransformer (Lee et al., 2019)	0.61	0.43	0.43	0.58	0.50	0.63
LieTransformer-T2 (Us)	0.87	0.87	0.80	0.87	0.79	0.84
LieTransformer-SE2 (Us)	0.85	0.85	0.85	0.85	0.85	0.85

Table 1. Test accuracies on the shape counting task at convergence

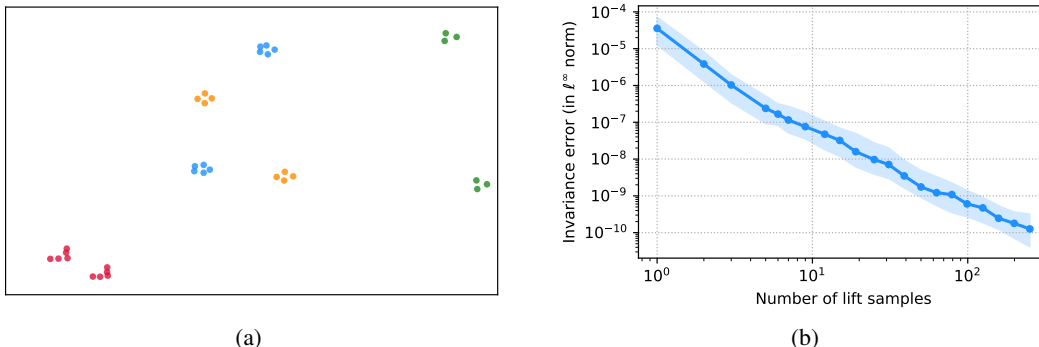


Figure 3. (a) An example 2D point cloud from D_{train} . The red, blue, yellow and green labels correspond to different patterns. (b) Invariance error vs. number of samples used in the Monte Carlo approximation during lifting for a single layer LieTransformer-SE2. The model outputs the logits over the shape classes which should be invariant to $SE(2)$ transformations of the input constellation. Plot shows median and interquartile range across 100 runs, randomizing over model seed, input constellation and transformation applied to input.

point.

We first create a fixed training set D_{train} and test set D_{test} of size 10,000 and 1,000 respectively. We then create augmented test sets D_{test}^{T2} and D_{test}^{SE2} that are copies of D_{test} with arbitrary transformations in $T(2)$ and $SE(2)$ respectively. In Table 1, we evaluate the test accuracy of LieTransformer at convergence with and without data augmentation during training time - D_{train}^{T2} and D_{train}^{SE2} indicate random $T(2)$ and $SE(2)$ augmentations respectively to each example of D_{train} at every training iteration. We compare against the baseline SetTransformer (Lee et al., 2019), a Transformer-based model that is permutation invariant, but not invariant to rotations nor translations. For LieTransformer, we consider the groups $T(2)$ and $SE(2)$ as the inputs are invariant to translations and rotations. We use roughly the same number of parameters for each model. See Appendix E.1 for further details on the setup.

Note that the test accuracy of LieTransformer-T2 remains unchanged when the train/test set is augmented with $T(2)$, and a similar story holds for LieTransformer-SE2 and $SE(2)$. On the other hand, the test accuracy of SetTransformer decreases with test set augmentation, whereas it increases with train set augmentation. Note that sometimes LieTransformer-T2 does slightly better than LieTransformer-SE2 on D_{test} and D_{test}^{T2} , most likely due to the fact that LieTransformer-SE2 is only $SE(2)$ -invariant in ex-

pectation (G_f is infinite since $H = SO(2)$), hence we need to subsample \hat{G}_f whereas LieTransformer-T2 is exactly $T(2)$ -invariant (G_f is infinite since $H = e$). However, we see that for D_{test}^{SE2} , LieTransformer-SE2 outperforms LieTransformer-T2, even with D_{train}^{SE2} . This shows the benefit of using an $SE(2)$ -invariant model over a $T(2)$ -invariant model with $SE(2)$ data augmentation.

In Figure 3b, we report the equivariance error of LieTransformer-SE2 when increasing the number of lift samples ($|\hat{H}|$) used in the Monte Carlo approximation of Equation 10. As expected, the invariance error decreases monotonically with the number of lift samples.

5.2. QM9: Molecular Property Regression from Molecular Geometry

We apply the LieTransformer to the QM9 molecule property prediction task (Wu et al., 2018). This dataset consists of 133,885 small inorganic molecules described by the location and charge of each atom in the molecule, along with the bonding structure of the molecule. The dataset includes 19 properties of each molecule, such as various rotational constants, energies and enthalpies, and 12 of these are used as regression tasks. We expect these molecular properties to be invariant to 3D roto-translations, i.e. $SE(3)$ -invariant.

In applying our model to this task, we ignore the bonding structure of the molecule. As noted in (Klicpera et al.,

Equivariant Self-Attention for Lie Groups

Task	α	$\Delta\epsilon$	ϵ_{HOMO}	ϵ_{LUMO}	μ	C_v	G	H	R^2	U	U_0	ZPVE
Units	bohr ³	meV	meV	meV	D	cal/mol K	meV	meV	bohr ²	meV	meV	meV
WaveScatt (Hirn et al., 2017)	.160	118	85	76	.340	.049	–	–	–	–	–	–
NMP (Gilmer et al., 2017)	.092	69	43	38	.030	.040	19	17	.180	20	20	1.50
SchNet (Schütt et al., 2017)	.235	63	41	34	.033	.033	14	14	.073	19	14	1.70
Cormorant (Anderson et al., 2019)	.085	61	34	38	.038	.026	20	21	.961	21	22	2.03
DimeNet (Klicpera et al., 2020)	.047	35	28	20	.029	.025	9	8	.331	7	8	1.29
L1Net (Miller et al., 2020)	.013	68	46	35	.009	.031	14	14	.099	13	13	1.56
TFN (Thomas et al., 2018)	.223	58	40	38	.064	.101	–	–	–	–	–	–
SE3-Transformer (Fuchs et al., 2020)	.148	53	36	33	.053	.057	–	–	–	–	–	–
LieConv-T3 (Finzi et al., 2020)	.125	60	36	32	.057	.046	35	37	1.54	36	35	3.62
LieConv-T3+SO3 Aug (Finzi et al., 2020)	.084	49	30	25	.032	.038	22	24	.800	19	19	2.28
LieConv-SE3+SO3 Aug (Finzi et al., 2020)	.088	45	27	25	.038	.043	47	46	2.12	44	45	3.25
LieTransformer-T3 (Us)	.179	67	47	37	.063	.046	27	29	.717	27	28	2.75
LieTransformer-T3+SO3 Aug (Us)	.082	51	33	27	.041	.035	19	17	.448	16	17	2.10
LieTransformer-SE3+SO3 Aug (Us)	.112	54	35	30	.066	.046	28	28	2.87	30	30	3.05

Table 2. QM9 molecular property prediction mean absolute error. Upper section of the table are non-equivariant models designed specifically for molecular property prediction, middle section are equivariant models designed specifically for molecular property prediction, lower section are general purpose equivariant models. Bold indicates best performance in a given section, underlined indicates best overall performance.

2020) this should not be needed to learn the task, although it may be helpful as auxiliary information. Given most methods compared against do not use such information, we follow this for a fair comparison (an exception is the $SE(3)$ -Transformer (Fuchs et al., 2020) that uses the bonding information). It would be possible to utilise the bonding structure both in the neighbourhood selection step and as model features by treating only atoms that are connected via a bond to another atom as in the neighbourhood of that atom.

We follow the customary practice of performing hyperparameter search on the ϵ_{HOMO} task and use the same hyperparameters for training on the other 11 tasks. Further details of the exact experimental setup can be found in Appendix E.2.

Table 2 shows the results of running our model on the 12 tasks. The results in Table 2 are broken into 3 sections. These detail models specifically designed to target the QM9 problem that are not equivariant, those that specifically target QM9 and are equivariant, and those that are general purpose equivariant models, applied to QM9. We show very competitive results, and perform best of generic equivariant methods on 8/12 tasks. In particular when comparing against LieConv, we see better performance on the majority of tasks, suggesting that the attention framework is better suited to this task than convolutions.

We trained three variants of both LieTransformer and LieConv. (1) $T(3)$ -equivariant model. (2) $T(3)$ -equivariant model trained with $SO(3)$ data augmentation.

(3) $SE(3)$ -equivariant (in expectation) model trained with $SO(3)$ data augmentation. Surprisingly we see that for both LieTransformer and LieConv the $T(3)$ model with $SO(3)$ augmentation outperforms the $SE(3)$ counterpart on most tasks. This is likely due to the Monte Carlo approximation of Equation 10 that only gives $SE(3)$ equivariance in expectation – the $SE(3)$ models were trained using $|\hat{H}| = 4$, and the variance of this estimate is likely causing imperfect equivariance and optimisation difficulties. Due to the $O(|G_f||nbhd_\eta|)$ memory cost for both LieTransformer and LieConv (Appendix D), we could not use a higher value of $|\hat{H}|$. Finding more memory-efficient ways to approximate Equation 10 or avoiding the sampling approximation would likely lead to improved results. Note however that LieTransformer-SE3 and LieConv-SE3 tend to outperform the irreducible representation (irrep) based $SE(3)$ -Transformer and TFN. This can be seen as further evidence that regular representation approaches tend to outperform irrep approaches, in line with the conclusions of Weiler & Cesa (2019).

5.3. Modelling Particle Trajectories with Hamiltonian Dynamics

We also apply the LieTransformer to a physics simulation task in the context of Hamiltonian dynamics. Hamiltonian mechanics is a formalism for describing the evolution of a physical system using a single scalar function, called the Hamiltonian. A notable fact about Hamiltonian dynamics is that symmetries of the Hamiltonian function play an

important role in the physical properties of the modelled system. Indeed, a famous result known as Noether’s theorem (Noether, 1971) states that if the Hamiltonian function has a symmetry, the resulting physical system modelled by the Hamiltonian will have a conserved quantity. For example, translation invariance of the Hamiltonian implies conservation of momentum and rotation invariance implies conservation of angular momentum. As conservation laws of a physical system are often known a priori, learning Hamiltonians with symmetries corresponding to these conservation laws would be useful for realistic modelling of particle trajectories.

For clarity, we consider the case of a single particle, although the Hamiltonian approach easily generalizes to an arbitrary number of particles. Consider a particle with position $\mathbf{q} \in \mathbb{R}^d$ and momentum $\mathbf{p} \in \mathbb{R}^d$ often compactly written as a single state $\mathbf{z} = (\mathbf{q}, \mathbf{p})$. We define a scalar function $H : \mathbb{R}^{2d} \rightarrow \mathbb{R}$ called the Hamiltonian, which takes as input the state of the particle and returns its total (potential plus kinetic) energy. The time evolution is then given by the following system of ODEs called Hamilton’s equations

$$\frac{d\mathbf{q}}{dt} = \frac{\partial H}{\partial \mathbf{p}}, \quad \frac{d\mathbf{p}}{dt} = -\frac{\partial H}{\partial \mathbf{q}}. \quad (12)$$

As a simple example, it is clear to see that translation invariance (in position) of the Hamiltonian implies conservation of momentum. Indeed, if $H(\mathbf{q}, \mathbf{p})$ is translation invariant then $\frac{\partial H}{\partial \mathbf{q}} = 0$ and so $\frac{d\mathbf{p}}{dt} = 0$, i.e. momentum is conserved. Noether’s theorem shows this in more generality: for any symmetry of the Hamiltonian there is a corresponding conserved quantity.

Several recent papers have considered modeling physical systems by learning the corresponding Hamiltonian of the system instead of learning the dynamics directly (Greydanus et al., 2019; Sanchez-Gonzalez et al., 2019; Zhong et al., 2019; Finzi et al., 2020). Specifically, we can parameterise the Hamiltonian by a neural network H_θ and learn the dynamics of the system by ensuring trajectories from the ground truth and learned system are close to each other. Given a learned H_θ , we can simulate the system for T timesteps by solving equation (12) with a numerical ODE solver to obtain a trajectory $\{\hat{\mathbf{z}}_t\}_{t=1}^T$ and minimize the difference between this trajectory and the ground truth $\{\mathbf{z}_t\}_{t=1}^T$:

$$L(\theta) = \frac{1}{T} \sum_{t=1}^T \|\hat{\mathbf{z}}_t - \mathbf{z}_t\|_2. \quad (13)$$

In our experiments, we parameterise the Hamiltonian H_θ by a LieTransformer and endow it with the symmetries corresponding to the conservation laws of the physical system we are modeling. We test our model on the spring dynamics task proposed in Sanchez-Gonzalez et al. (2019).

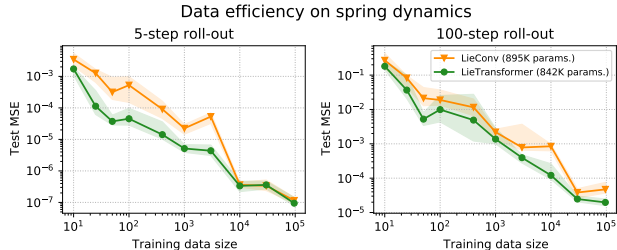


Figure 4. Data efficiency of models on Hamiltonian spring dynamics. Both models are trained using 5-step roll-outs. The left and right plot shows test performance with 5-step and 100-step roll-outs respectively. Plots show median MSE and interquartile range across 10 model seeds.

Specifically, we consider a system of n particles with mass m_1, \dots, m_n in two dimensions with each particle connected to all others by springs. This system conserves both linear and angular momentum, so the ground truth Hamiltonian will be both translationally and rotationally invariant. We simulate this system for 500 timesteps from various initial conditions and use random subsets of these roll-outs to train the model (see Appendix E.3 for full experimental details).

As approaches that explicitly take the symmetries of the Hamiltonian into account have been shown to outperform ones that don’t (Finzi et al., 2020), we only compare our method to LieConv. Figure 4 shows the performance of our model as a function of the number of training points. As can be seen, the model is highly data-efficient: the inductive bias from the symmetries of the Hamiltonian allow us to accurately learn the dynamics even from a small training set. Further, our model consistently performs better than LieConv suggesting that the attention framework is also useful for this task. In addition, the invariance of the LieTransformer model improves generalization: even though we only train on 5-step roll-outs, our model generalizes well to 100-step roll-outs.

Figure 5 shows the test error as function of the roll-out time step for a training data size of 10,000 (corresponding plots for other training data sizes are included in the appendix). As expected, the difference between the ground truth and predicted trajectories increases with time although the error remains low ($< 10^{-3}$ after 100 time steps). Further, the LieTransformer model consistently outperforms LieConv. We also include example trajectories of our model in Figure 6 (more examples can be found in the appendix, including ones where LieConv performs better than LieTransformer) illustrating the accuracy of our model on this task.

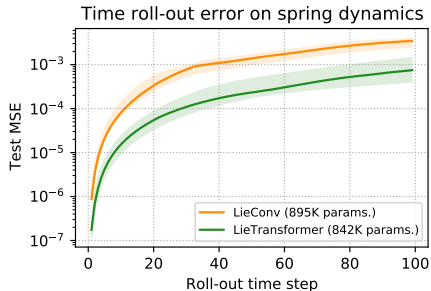


Figure 5. Test error vs. roll-out time step. The training data size is 10,000 for both models. Plots show median MSE and interquartile range across 10 model seeds.

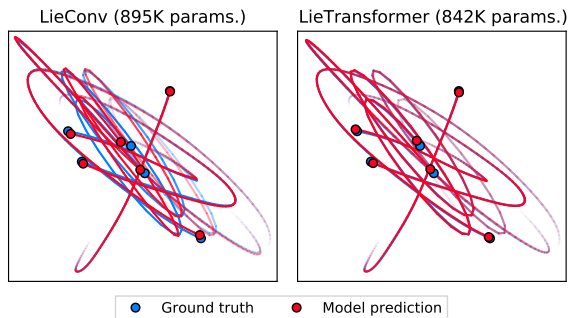


Figure 6. Example trajectories of our model on the spring dynamics task. As can be seen our model closely follows the ground truth while the LieConv model diverges from the ground truth at later timesteps.

6. Limitations and Future Work

From the algorithmic perspective, `LieTransformer` shares the weakness of `LieConv` in being memory-expensive due to: 1. The lifting procedure that increases the number of inputs by $|\hat{H}|$, and 2. Quadratic complexity in the number of inputs from having to compute the kernel value at each pair of inputs. Although the first cause is a weakness shared by all lifting-based equivariant neural networks, the second cause can be addressed by incorporating works that study efficient variants of self-attention (Wang et al., 2020; Kitaev et al., 2020; Zaheer et al., 2020; Katharopoulos et al., 2020). An alternative approach is to incorporate information about pairs of inputs (such as bonding information for the QM9 task) as masking in self-attention.

From the methodological perspective, a key weakness of the `LieTransformer` that is also shared with `LieConv` is its approximate equivariance due to MC estimation of the integral in Equation 10 for the case where H is infinite. The aforementioned directions for memory-efficiency can help to reduce the approximation error by allowing to use more samples after lifting (higher $|\hat{H}|$). An alternative would be to use Fast Fourier Transforms to approximate the integral

as in Cohen et al. (2018). Other further directions include incorporating the notion of *steerability* (Cohen & Welling, 2016b) to deal with vector fields in an equivariant manner (given inputs (x_i, \mathbf{f}_i) , the group acts non-trivially on \mathbf{f}_i as well as x_i), and extending to non-homogeneous input spaces as outlined in Finzi et al. (2020).

ACKNOWLEDGEMENTS

The authors would like to thank Adam R. Kosiorek for setting up the initial codebase at the beginning of the project, and David W. Romero & Jean-Baptiste Cordonnier for useful discussions. Michael is supported by the EPSRC Centre for Doctoral Training in Modern Statistics and Statistical Machine Learning (EP/S023151/1). Charline acknowledges funding from the EPSRC grant agreement no. EP/N509711/1. Sheheryar wishes to acknowledge support from Aker Scholarship. Emilien acknowledges support of his PhD funding from Google DeepMind. Yee Whye Teh’s research leading to these results has received funding from the European Research Council under the European Union’s Seventh Framework Programme (FP7/2007-2013) ERC grant agreement no. 617071.

We would also like to thank the Python community (Van Rossum & Drake Jr, 1995; Oliphant, 2007) for developing the tools that enabled this work, including PyTorch (Paszke et al., 2017), NumPy (Oliphant, 2006; Walt et al., 2011; Harris et al., 2020), SciPy (Jones et al., 2001), and Matplotlib (Hunter, 2007).

References

- Anderson, B., Hy, T. S., and Kondor, R. Cormorant: Covariant molecular neural networks. In *Advances in Neural Information Processing Systems*, pp. 14537–14546, 2019.
- Ba, J. L., Kiros, J. R., and Hinton, G. E. Layer normalization. *arXiv preprint arXiv:1607.06450*, 2016.
- Bekkers, E. J. B-spline CNNs on Lie groups. In *International Conference on Learning Representations*, 2020.
- Bloem-Reddy, B. and Teh, Y. W. Probabilistic symmetry and invariant neural networks. *arXiv preprint arXiv:1901.06082*, 2019.
- Brown, T. B., Mann, B., Ryder, N., Subbiah, M., Kaplan, J., Dhariwal, P., Neelakantan, A., Shyam, P., Sastry, G., Askell, A., et al. Language models are few-shot learners. *arXiv preprint arXiv:2005.14165*, 2020.
- Cohen, T. and Welling, M. Group equivariant convolutional networks. In *International conference on machine learning*, pp. 2990–2999, 2016a.
- Cohen, T. S. and Welling, M. Steerable CNNs. *arXiv preprint arXiv:1612.08498*, 2016b.

- Cohen, T. S., Geiger, M., Köhler, J., and Welling, M. Spherical CNNs. In *International Conference on Learning Representations (ICLR)*, 2018.
- Cohen, T. S., Geiger, M., and Weiler, M. A general theory of equivariant CNNs on homogeneous spaces. In *Advances in Neural Information Processing Systems*, pp. 9142–9153, 2019.
- Dosovitskiy, A., Beyer, L., Kolesnikov, A., Weissenborn, D., Zhai, X., Unterthiner, T., Dehghani, M., Minderer, M., Heigold, G., Gelly, S., et al. An image is worth 16x16 words: Transformers for image recognition at scale. *arXiv preprint arXiv:2010.11929*, 2020.
- Esteves, C. Theoretical aspects of group equivariant neural networks. *arXiv preprint arXiv:2004.05154*, 2020.
- Esteves, C., Allen-Blanchette, C., Makadia, A., and Daniilidis, K. Learning SO(3) equivariant representations with spherical CNNs. In *Proceedings of the European Conference on Computer Vision (ECCV)*, pp. 52–68, 2018.
- Esteves, C., Makadia, A., and Daniilidis, K. Spin-weighted spherical CNNs. *arXiv preprint arXiv:2006.10731*, 2020.
- Finzi, M., Stanton, S., Izmailov, P., and Wilson, A. G. Generalizing convolutional neural networks for equivariance to Lie groups on arbitrary continuous data. *arXiv preprint arXiv:2002.12880*, 2020.
- Fuchs, F. B., Worrall, D. E., Fischer, V., and Welling, M. SE(3)-Transformers: 3D roto-translation equivariant attention networks. *arXiv preprint arXiv:2006.10503*, 2020.
- Gilmer, J., Schoenholz, S. S., Riley, P. F., Vinyals, O., and Dahl, G. E. Neural message passing for quantum chemistry. *arXiv preprint arXiv:1704.01212*, 2017.
- Graves, A. and Jaitly, N. Towards end-to-end speech recognition with recurrent neural networks. In *International conference on machine learning*, pp. 1764–1772, 2014.
- Greydanus, S., Dzamba, M., and Yosinski, J. Hamiltonian neural networks. *arXiv preprint arXiv:1906.01563*, 2019.
- Harris, C. R., Millman, K. J., van der Walt, S. J., Gommers, R., Virtanen, P., Cournapeau, D., Wieser, E., Taylor, J., Berg, S., Smith, N. J., et al. Array programming with numpy. *Nature*, 585(7825):357–362, 2020.
- Hirn, M., Mallat, S., and Poilvert, N. Wavelet scattering regression of quantum chemical energies. *Multiscale Modeling & Simulation*, 15(2):827–863, 2017.
- Hoogeboom, E., Peters, J. W., Cohen, T. S., and Welling, M. HexaConv. In *International Conference on Learning Representations*, 2018.
- Huang, C.-Z. A., Vaswani, A., Uszkoreit, J., Simon, I., Hawthorne, C., Shazeer, N., Dai, A. M., Hoffman, M. D., Dinculescu, M., and Eck, D. Music Transformer. In *International Conference on Learning Representations*, 2019.
- Hunter, J. D. Matplotlib: A 2d graphics environment. *Computing in science & engineering*, 9(3):90–95, 2007.
- Ioffe, S. and Szegedy, C. Batch normalization: Accelerating deep network training by reducing internal covariate shift. *arXiv preprint arXiv:1502.03167*, 2015.
- Jones, E., Oliphant, T., Peterson, P., et al. Scipy: Open source scientific tools for python. 2001.
- Katharopoulos, A., Vyas, A., Pappas, N., and Fleuret, F. Transformers are rnns: Fast autoregressive transformers with linear attention. In *International Conference on Machine Learning*, pp. 5156–5165. PMLR, 2020.
- Kingma, D. P. and Ba, J. Adam: A method for stochastic optimization. *arXiv preprint arXiv:1412.6980*, 2014.
- Kitaev, N., Kaiser, Ł., and Levskaya, A. Reformer: The efficient transformer. *arXiv preprint arXiv:2001.04451*, 2020.
- Klicpera, J., Groß, J., and Günnemann, S. Directional message passing for molecular graphs. *arXiv preprint arXiv:2003.03123*, 2020.
- Kondor, R. and Trivedi, S. On the generalization of equivariance and convolution in neural networks to the action of compact groups. In *International Conference on Machine Learning*, pp. 2747–2755, 2018.
- Kondor, R., Lin, Z., and Trivedi, S. Clebsch–Gordan nets: a fully Fourier space spherical convolutional neural network. In *Advances in Neural Information Processing Systems*, pp. 10117–10126, 2018.
- Kosioerek, A., Sabour, S., Teh, Y. W., and Hinton, G. E. Stacked capsule autoencoders. In *Advances in Neural Information Processing Systems*, pp. 15512–15522, 2019.
- Krizhevsky, A., Sutskever, I., and Hinton, G. E. Imagenet classification with deep convolutional neural networks. In *Advances in neural information processing systems*, pp. 1097–1105, 2012.
- Lee, J., Lee, Y., Kim, J., Kosioerek, A., Choi, S., and Teh, Y. W. Set transformer: A framework for attention-based permutation-invariant neural networks. volume 97 of *Proceedings of Machine Learning Research*. PMLR, 09–15 Jun 2019. URL <http://proceedings.mlr.press/v97/lee19d.html>.

- Miller, B. K., Geiger, M., Smidt, T. E., and Noé, F. Relevance of rotationally equivariant convolutions for predicting molecular properties. *arXiv preprint arXiv:2008.08461*, 2020.
- Noether, E. Invariant variation problems. *Transport Theory and Statistical Physics*, 1(3):186–207, 1971.
- Oliphant, T. E. *A guide to NumPy*, volume 1. Trelgol Publishing USA, 2006.
- Oliphant, T. E. Python for scientific computing. *Computing in Science & Engineering*, 9(3):10–20, 2007.
- Parisotto, E., Song, H. F., Rae, J. W., Pascanu, R., Gulcehre, C., Jayakumar, S. M., Jaderberg, M., Kaufman, R. L., Clark, A., Noury, S., Botvinick, M. M., Heess, N., and Hadsell, R. Stabilizing Transformers for reinforcement learning. In *International Conference on Machine Learning*, 2020.
- Parmar, N., Ramachandran, P., Vaswani, A., Bello, I., Levskaya, A., and Shlens, J. Stand-alone self-attention in vision models. In Wallach, H., Larochelle, H., Beygelzimer, A., Alché-Buc, F., Fox, E., and Garnett, R. (eds.), *Advances in Neural Information Processing Systems 32*, pp. 68–80. Curran Associates, Inc., 2019a.
- Parmar, N., Ramachandran, P., Vaswani, A., Bello, I., Levskaya, A., and Shlens, J. Stand-alone self-attention in vision models. In *Advances in Neural Information Processing Systems*, pp. 68–80, 2019b.
- Paszke, A., Gross, S., Chintala, S., Chanan, G., Yang, E., DeVito, Z., Lin, Z., Desmaison, A., Antiga, L., and Lerer, A. Automatic differentiation in pytorch. 2017.
- Romero, D. W. and Cordonnier, J.-B. Group equivariant stand-alone self-attention for vision. *arXiv preprint arXiv:2010.00977*, 2020.
- Romero, D. W., Bekkers, E. J., Tomczak, J. M., and Hoogenboom, M. Attentive group equivariant convolutional networks. *arXiv preprint arXiv:2002.03830*, 2020.
- Sanchez-Gonzalez, A., Bapst, V., Cranmer, K., and Battaglia, P. Hamiltonian graph networks with ode integrators. *arXiv preprint arXiv:1909.12790*, 2019.
- Schütt, K., Kindermans, P.-J., Felix, H. E. S., Chmiela, S., Tkatchenko, A., and Müller, K.-R. SchNet: A continuous-filter convolutional neural network for modeling quantum interactions. In *Advances in neural information processing systems*, pp. 991–1001, 2017.
- Thomas, N., Smidt, T., Kearnes, S., Yang, L., Li, L., Kohlhoff, K., and Riley, P. Tensor field networks: Rotation-and translation-equivariant neural networks for 3D point clouds. *arXiv preprint arXiv:1802.08219*, 2018.
- Tsai, Y.-H. H., Bai, S., Yamada, M., Morency, L.-P., and Salakhutdinov, R. Transformer dissection: An unified understanding for Transformer’s attention via the lens of kernel. In *Proceedings of the 2019 Conference on Empirical Methods in Natural Language Processing and the 9th International Joint Conference on Natural Language Processing*, pp. 4344–4353, 2019.
- Van Rossum, G. and Drake Jr, F. L. *Python reference manual*. Centrum voor Wiskunde en Informatica Amsterdam, 1995.
- Vaswani, A., Shazeer, N., Parmar, N., Uszkoreit, J., Jones, L., Gomez, A. N., Kaiser, L., and Polosukhin, I. Attention is all you need. In Guyon, I., Luxburg, U. V., Bengio, S., Wallach, H., Fergus, R., Vishwanathan, S., and Garnett, R. (eds.), *Advances in Neural Information Processing Systems 30*, pp. 5998–6008. Curran Associates, Inc., 2017. URL <http://papers.nips.cc/paper/7181-attention-is-all-you-need.pdf>.
- Walt, S. v. d., Colbert, S. C., and Varoquaux, G. The numpy array: a structure for efficient numerical computation. *Computing in science & engineering*, 13(2):22–30, 2011.
- Wang, S., Li, B., Khabsa, M., Fang, H., and Ma, H. Linformer: Self-attention with linear complexity. *arXiv preprint arXiv:2006.04768*, 2020.
- Wang, X., Girshick, R., Gupta, A., and He, K. Non-local neural networks. In *Proceedings of the IEEE Conference on Computer Vision and Pattern Recognition*, pp. 7794–7803, 2018.
- Weiler, M. and Cesa, G. General E(2)-equivariant steerable CNNs. In *Advances in Neural Information Processing Systems*, pp. 14334–14345, 2019.
- Weiler, M., Geiger, M., Welling, M., Boomsma, W., and Cohen, T. S. 3D steerable CNNs: Learning rotationally equivariant features in volumetric data. In *Advances in Neural Information Processing Systems*, pp. 10381–10392, 2018a.
- Weiler, M., Hamprecht, F. A., and Storath, M. Learning steerable filters for rotation equivariant CNNs. In *Proceedings of the IEEE Conference on Computer Vision and Pattern Recognition*, pp. 849–858, 2018b.
- Worrall, D. E., Garbin, S. J., Turmukhambetov, D., and Brostow, G. J. Harmonic networks: Deep translation and rotation equivariance. In *Proceedings of the IEEE Conference on Computer Vision and Pattern Recognition*, pp. 5028–5037, 2017.
- Wu, Z., Ramsundar, B., Feinberg, E. N., Gomes, J., Geniesse, C., Pappu, A. S., Leswing, K., and Pande, V. MoleculeNet: a benchmark for molecular machine learning. *Chemical science*, 9(2):513–530, 2018.

Zaheer, M., Guruganesh, G., Dubey, K. A., Ainslie, J., Alberti, C., Ontanon, S., Pham, P., Ravula, A., Wang, Q., Yang, L., et al. Big bird: Transformers for longer sequences. *Advances in Neural Information Processing Systems*, 33, 2020.

Zhang, H., Goodfellow, I., Metaxas, D., and Odena, A. Self-attention Generative Adversarial Networks. In *Proceedings of the 36th International Conference on Machine Learning*, pp. 7354–7363, 2019.

Zhong, Y. D., Dey, B., and Chakraborty, A. Symplectic ode-net: Learning hamiltonian dynamics with control. *arXiv preprint arXiv:1909.12077*, 2019.

Appendix

A. Contributions

- Charline and Yee Whye conceived the project and Yee Whye initially came up with an equivariant form of self-attention.
- Through discussions between Michael, Charline, Hyunjik and Yee Whye, this was modified to the current `LieSelfAttention` layer, and Michael derived the equivariance of the `LieSelfAttention` layer.
- Michael, Sheheryar and Hyunjik simplified the proof of equivariance and further developed the methodology for the `LieTransformer` in its current state, and created links between `LieTransformer` and other related work.
- Michael wrote the initial framework of the `LieTransformer` codebase. Charline and Sheheryar wrote the code for the shape counting experiments, Michael wrote the code for the QM9 experiments, Sheheryar wrote the code for the Hamiltonian dynamics experiments, after helpful discussions with Emilien.
- Charline carried out the experiments for Table 1, Michael carried out most of the experiments for Table 2 with some help from Hyunjik, Sheheryar carried out the experiments for Figure 3b and all the Hamiltonian dynamics experiments.
- Hyunjik wrote all sections of the paper except the experiment sections: the shape counting section was written by Charline, the QM9 section by Michael and the Hamiltonian dynamics section was written by Emilien and Sheheryar.

B. Proofs

Lemma 1. *The function composition $f \circ f_K \circ \dots \circ f_1$ of several equivariant functions f_k , $k \in \{1, 2, \dots, K\}$ followed by an invariant function f , is an invariant function.*

Proof. Consider group representations π_1, \dots, π_K that act on f_1, \dots, f_K respectively, and representation π_0 that acts on the input space of f_1 . If each f_k is equivariant with respect to π_k, π_{k-1} such that $f_k \circ \pi_{k-1} = \pi_k \circ f_k$, and f is invariant such that $f \circ \pi_k = f$, then we have

$$\begin{aligned} f \circ f_k \circ \dots \circ f_1 \circ \pi_0 &= f \circ f_k \circ \dots \circ \pi_1 \circ f_1 \\ &\vdots \\ &= f \circ \pi_k \circ f_k \circ \dots \circ f_1 \\ &= f \circ f_k \circ \dots \circ f_1, \end{aligned}$$

hence $f \circ f_k \circ \dots \circ f_1$ is invariant. \square

Lemma 2. *The group equivariant convolution $\Psi : \mathcal{I}_U \rightarrow \mathcal{I}_U$ defined as: $[\Psi f](g) \triangleq \int_G \psi(g'^{-1}g)f(g')dg'$ is equivariant with respect to the regular representation π of G acting on \mathcal{I}_U as $[\pi(u)f](g) \triangleq f(u^{-1}g)$.*

Proof.

$$\begin{aligned} \Psi[\pi(u)f](g) &= \int_G \psi(g'^{-1}g)[\pi(u)f](g')dg' \\ &= \int_{uG} \psi(g'^{-1}g)f(u^{-1}g')dg' \\ &= \int_G \psi(g'^{-1}u^{-1}g)f(g')dg' \\ &= [\Psi f](u^{-1}g) \\ &= [\pi(u)[\Psi f]](g). \end{aligned}$$

The second equality holds by invariance of the left Haar measure. \square

Proposition 1. *The lifting layer \mathcal{L} is equivariant with respect to the representation π .*

Proof. • $\mathcal{L}[\pi(u)f_{\mathcal{X}}](g) = \mathbf{f}_i$ for $g \in s(ux_i)H$.

• $[\pi(u)\mathcal{L}[f_{\mathcal{X}}]](g) = \mathcal{L}[f_{\mathcal{X}}](u^{-1}g) = \mathbf{f}_i$ for $g \in us(x_i)H$.

• $s(ux_i)H = us(x_i)H \forall u \in G$.

□

Proposition 2. *LieSelfAttention is equivariant with respect to the regular representation π .*

Proof. Let $\mathcal{I}_U = \mathcal{L}(G, \mathbb{R}^D)$ be the space of unconstrained functions $f : G \rightarrow \mathbb{R}^D$. We can define the regular representation π of G acting on \mathcal{I}_U as follows:

$$[\pi(u)f](g) = f(u^{-1}g) \quad (14)$$

f is defined on the set $G_f = \cup_{i=1}^n s(x_i)H$ (i.e. union of cosets corresponding to each x_i). Note $G_{\pi(u)f} = uG_f$, and G_f does not depend on the choice of section s .

Note that for all above choices of k_c and k_l , we have:

$$k_c([\pi(u)f](g), [\pi(u)f](g')) = k_c(f(u^{-1}g), f(u^{-1}g')) \quad (15)$$

$$k_l(g^{-1}g') = k_l((u^{-1}g)^{-1}(u^{-1}g')) \quad (16)$$

Hence for all choices of F , we have that

$$\begin{aligned} \alpha_{\pi(u)f}(g, g') &= F(k_c([\pi(u)f](g), [\pi(u)f](g')), k_l(g^{-1}g')) \\ &= F(k_c(f(u^{-1}g), f(u^{-1}g')), k_l((u^{-1}g)^{-1}u^{-1}g')) \\ &= \alpha_f(u^{-1}g, u^{-1}g') \end{aligned} \quad (17)$$

We thus prove equivariance for the below choice of `LieSelfAttention` $\Phi : \mathcal{I}_U \rightarrow \mathcal{I}_U$ that uses softmax normalisation, but a similar proof holds for constant normalisation. Let $A_f(g, g') \triangleq \exp(\alpha_f(g, g'))$, hence Equation (17) also holds for A_f .

$$[\Phi f](g) = \int_{G_f} w_f(g, g') f(g') dg' \quad (18)$$

$$= \int_{G_f} \frac{A_f(g, g')}{\int_{G_f} A_f(g, g'') dg''} f(g') dg' \quad (19)$$

Hence:

$$\begin{aligned} w_{\pi(u)f}(g, g') &= \frac{A_{\pi(u)f}(g, g')}{\int_{G_{\pi(u)f}} A_{\pi(u)f}(g, g'') dg''} \\ &= \frac{A_f(u^{-1}g, u^{-1}g')}{\int_{uG_f} A_f(u^{-1}g, u^{-1}g'') dg''} \\ &= \frac{A_f(u^{-1}g, u^{-1}g')}{\int_{G_f} A_f(u^{-1}g, g'') dg''} \\ &= w_f(u^{-1}g, u^{-1}g') \end{aligned} \quad (20)$$

Then we can show that Φ is equivariant with respect to the representation π as follows:

$$\begin{aligned}
 \Phi[\pi(u)f](g) &= \int_{G_{\pi(u)f}} w_{\pi(u)f}(g, g') [\pi(u)f](g') dg' \\
 &= \int_{uG_f} w_f(u^{-1}g, u^{-1}g') f(u^{-1}g') dg' \\
 &= \int_{G_f} w_f(u^{-1}g, g') f(g') dg' \\
 &= [\Phi f](u^{-1}g) \\
 &= [\pi(u)[\Phi f]](g)
 \end{aligned} \tag{21}$$

□

Equivariance holds for any α_f that satisfies Equation (17). Multiplying α_f by an indicator function $\mathbb{1}\{d(g, g') < \lambda\}$ where $d(g, g')$ is some function of $g^{-1}g'$, we can show that *local* self-attention that restricts attention to points in a neighbourhood also satisfies equivariance. When approximating the integral with Monte Carlo samples (equivalent to replacing G_f with \hat{G}_f) we obtain a self-attention layer that is equivariant in expectation for constant normalisation of attention weights (i.e. $\mathbb{E}[\hat{\Phi}[\pi(u)f](g)] = \Phi[\pi(u)f](g) = \Phi[\pi(u)f](g)$ where $\hat{\Phi}$ is the same as Φ but with \hat{G}_f instead of G_f). However for softmax normalisation we obtain a biased estimate due to the nested MC estimate in the denominator's normalising constant.

C. Log map formulas for Lie groups

- $G = T(n), t \in \mathbb{R}^n, \nu[\log(t)] = t$

- $G = SO(2), R = \begin{bmatrix} \cos \theta & -\sin \theta \\ \sin \theta & \cos \theta \end{bmatrix} \in \mathbb{R}^{2 \times 2}$

$$\nu[\log(R)] = \theta = \arctan(R_{10}/R_{01}) \tag{22}$$

- $G = SE(2), R = \begin{bmatrix} \cos \theta & -\sin \theta \\ \sin \theta & \cos \theta \end{bmatrix} \in \mathbb{R}^{2 \times 2}, t \in \mathbb{R}^2$

$$\nu[\log(tR)] = \begin{bmatrix} t' \\ \theta \end{bmatrix} \tag{23}$$

where $t' = V^{-1}t, V = \begin{bmatrix} a & -b \\ b & a \end{bmatrix}, a \triangleq \frac{\sin \theta}{\theta}, b \triangleq \frac{1 - \cos \theta}{\theta}$

- $G = SO(3), R \in \mathbb{R}^{3 \times 3}, t \in \mathbb{R}^3:$

$$\nu[\log(R)] = \nu \left[\frac{\theta}{2 \sin \theta} (R - R^\top) \right] = \frac{\theta}{2 \sin \theta} \begin{bmatrix} R_{21} - R_{12} \\ R_{02} - R_{20} \\ R_{10} - R_{01} \end{bmatrix} \tag{24}$$

where $\cos \theta = \frac{\text{Tr}(R) - 1}{2}$. Note that the Taylor expansion of $\theta / \sin \theta$ should be used when θ is small.

- $G = SE(3), R \in \mathbb{R}^{3 \times 3}, t \in \mathbb{R}^3:$

$$\nu[\log(tR)] = \begin{bmatrix} t' \\ r' \end{bmatrix} \tag{25}$$

where $t' = V^{-1}t, r' = \nu[\log(R)], V = I + \frac{1 - \cos \theta}{\theta^2} (R - R^\top) + \frac{\theta - \sin \theta}{\theta^3} (R - R^\top)^2$.

D. Memory and Time Complexity Comparison with LieConv

D.1. LieConv

- Inputs: $\{g, f(g)\}_{g \in G_f}$ where
 - $f(g) \in \mathbb{R}^{d_v}$
 - G_f defined as in Section 3.1.
- Outputs: $\{g, \frac{1}{|\text{nbhd}(g)|} \sum_{g' \in \text{nbhd}(g)} k_L(g^{-1}g')f(g')\}_{g \in G_f}$ where
 - $\text{nbhd}(g) = \{g' \in G_f : \nu[\log(g)] < r\}$. Let us assume that $|\text{nbhd}(g)| \approx n \forall g$.
 - $k_L(g^{-1}g') = \text{MLP}_\theta(\nu[\log(g^{-1}g')]) \in \mathbb{R}^{d_{out} \times d_v}$.

There are (at least) two ways of computing LieConv: 1. Naive and 2. PointConv Trick.

1. Naive

- **Memory:** Store $k_L(g^{-1}g') \in \mathbb{R}^{d_{out} \times d_v} \forall g \in G_f, g' \in \text{nbhd}(g)$. This requires $O(|G_f|nd_{out}d_v)$ memory.
- **Time:** Compute $k_L(g^{-1}g')f(g') \forall g \in G_f, g' \in \text{nbhd}(g)$. This requires $O(|G_f|nd_{out}d_v)$ flops.

2. PointConv Trick

One-line summary: instead of applying a shared linear map then summing across nbhd, first sum across nbhd then apply the linear map.

Details: $k_L(g^{-1}g') = \text{MLP}_\theta(\nu[\log(g^{-1}g')]) = \text{reshape}(HM(g^{-1}g'), [d_{out}, d_v])$ where

- $M(g^{-1}g') \in \mathbb{R}^{d_{mid}}$ are the final layer activations of MLP_θ .
- $H \in \mathbb{R}^{d_{out}d_v \times d_{mid}}$ is the final linear layer of MLP_θ .

The trick assumes $d_{mid} \ll d_{out}d_v$, and reorders the computation as:

$$\begin{aligned} & \sum_{g' \in \text{nbhd}(g)} \text{reshape}(HM(g^{-1}g'), [d_{out}, d_v])f(g') \\ &= \text{reshape}(H, [d_{out}, d_v d_{mid}]) \sum_{g' \in \text{nbhd}(g)} M(g^{-1}g') \otimes f(g') \end{aligned}$$

where \otimes is the Kronecker product: $x \otimes y = [x_1y_1, \dots, x_1y_{d_y}, \dots, x_{d_x}y_1, \dots, x_{d_x}y_{d_y}] \in \mathbb{R}^{d_x d_y}$. So $M(g^{-1}g') \otimes f(g') \in \mathbb{R}^{d_v d_{mid}}$.

- **Memory:** Store $M(g^{-1}g') \forall g \in G_f, g' \in \text{nbhd}(g)$, and store H . This requires $O(|G_f|nd_{mid} + d_{out}d_v d_{mid})$ memory.

- **Time:** Compute $\sum_{g' \in \text{nbhd}(g)} M(g^{-1}g') \otimes f(g')$ via matrix multiplication:

$$\begin{bmatrix} | & & | \\ M(g^{-1}g'_1) & \dots & M(g^{-1}g'_n) \\ | & & | \end{bmatrix} \begin{bmatrix} - & f(g'_1) & - \\ \vdots & & \\ - & f(g'_n) & - \end{bmatrix}. \text{ This requires } O(d_v n d_{mid}) \text{ flops.}$$

Then multiply by H , requiring $O(d_v d_{out} d_{mid})$ flops.

This is done for each $g \in G_f$, so the total number of flops is $O(|G_f|d_v d_{mid}(n + d_{out}))$.

D.2. Equivariant Self-Attention

- Inputs: $\{g, f(g)\}_{g \in G_f}$ where
 - $f(g) \in \mathbb{R}^{d_v}$
 - G_f defined as in Section 3.1.
- Outputs: $\{g, f(g) + \sum_{g' \in \text{nbhd}(g)} w_f(g, g')W^V f(g')\}_{g \in G_f}$ where

- $\text{nbhd}(g) = \{g' \in G_f : \nu[\log(g)] < r\}$. Let us assume that $|\text{nbhd}(g)| \approx n \forall g$.
- $\{w_f(g, g')\}_{g' \in G_f} = \text{softmax}(\{\alpha_f(g, g')\}_{g' \in G_f})$
- $\alpha_f(g, g') = k_f(f(g), f(g')) + k_x(g^{-1}g')$
- $k_f(f(g), f(g')) = (W^Q f(g))^\top W^K f(g') \in \mathbb{R}$
- $k_x(g) = \text{MLP}_\phi(\nu[\log(g)]) \in \mathbb{R}$
- $W^Q, W^K, W^V \in \mathbb{R}^{d_v \times d_v}$.

- **Memory:** Store $\alpha_f(g, g')$ and $W^V f(g') \forall g \in G_f, g' \in \text{nbhd}(g)$. This requires $O(|G_f|nd_v)$ memory.
- **Time:** Compute $k_f(f(g), f(g'))$ and $w_f(g, g') \forall g \in G_f, g' \in \text{nbhd}(g)$. This requires $O(|G_f|nd_v^2)$ flops.

With multihead self-attention (M heads), the output is:

$$f(g) + W^O \begin{bmatrix} V^1 \\ \vdots \\ V^M \end{bmatrix}$$

where $W^O \in \mathbb{R}^{d_v \times d_v}$, $V^m = \sum_{g' \in \text{nbhd}(g)} w_f(g, g') W^{V,m} f(g')$ for $W^{K,m}, W^{Q,m}, W^{V,m} \in \mathbb{R}^{d_v/M \times d_v}$.

- **Memory:** Store $\alpha_f^m(g, g')$ and $W^{V,m} f(g') \forall g \in G_f, g' \in \text{nbhd}(g), m \in \{1, \dots, M\}$. This requires $O(M|G_f|n + M|G_f|nd_v/M) = O(|G_f|n(M + d_v))$ memory.
- **Time:** Compute $k_f^m(f(g), f(g'))$ and $w_f^m(g, g') \forall g \in G_f, g' \in \text{nbhd}(g), m \in \{1, \dots, M\}$. This requires $O(M|G_f|nd_v d_v/M) = O(|G_f|nd_v^2)$ flops.

E. Other Equivariant/Invariant building blocks

G-Pooling is simply averaging over the features across the group: Inputs: $\{f(g)\}_{g \in G_f}$ Output: $\bar{f}(g) \triangleq \frac{1}{|G_f|} \sum_{g \in G_f} f(g)$
Note that G-pooling is invariant with respect to the regular representation.

Pointwise MLPs are MLPs applied independently to each $f(g)$ for $g \in G_f$. It is easy to show that any such pointwise operations are equivariant with respect to the regular representation.

LayerNorm (Ba et al., 2016) is defined as follows:

Inputs: $\{g, f(g)\}_{g \in G_f}$ where

- $f(g) \in \mathbb{R}^{d_v}$
- G_f defined as in Section 3.1.

Outputs: $\{g, \beta \odot \frac{f(g) - m(g)}{\sqrt{v(g) + \epsilon}} + \gamma\}_{g \in G_f}$ where

- Division in fraction above is *scalar* division i.e. $\sqrt{v(g) + \epsilon} \in \mathbb{R}$.
- $m(g) = \text{Mean}_c f_c(g') \in \mathbb{R}$.
- $v(g) = \text{Var}_c f_c(g') \in \mathbb{R}$.
- $\beta, \gamma \in \mathbb{R}^D$ are learnable parameters.

BatchNorm We also describe BatchNorm (Ioffe & Szegedy, 2015) that is used in (Finzi et al., 2020) for completeness:

Inputs: $\{g, f^b(g)\}_{g \in G_f, b \in B}$ where

- $f(g) \in \mathbb{R}^{d_v}$
- G_f defined as in Section 3.1, \mathcal{B} is the batch of examples.

Outputs: $\{g, \beta \odot \frac{f^b(g) - \mathbf{m}(g)}{\sqrt{\mathbf{v}(g) + \epsilon}} + \gamma\}_{g \in G_f, b \in \mathcal{B}}$ where

- Division in fraction above denotes *pointwise* division i.e. $\sqrt{\mathbf{v}(g) + \epsilon} \in \mathbb{R}^D$.
- $\mathbf{m}(g) = \text{Mean}_{g' \in \text{nbhd}(g), b \in \mathcal{B}} f^b(g') \in \mathbb{R}^D$ - Mean is taken for every channel.
- $\mathbf{v}(g) = \text{Var}_{g' \in \text{nbhd}(g), b \in \mathcal{B}} f^b(g') \in \mathbb{R}^D$ - Var is taken for every channel.
- $\text{nbhd}(g) = \{g' \in G_f : \nu[\log(g)] < r\}$.
- $\beta, \gamma \in \mathbb{R}^D$ are learnable parameters.

A moving average of $\mathbf{m}(g)$ and $\mathbf{v}(g)$ are tracked during training time for use at test time. It is easy to check that both BatchNorm and LayerNorm are equivariant wrt the action of the regular representation π on f (for BatchNorm, note $g' \in \text{nbhd}(g)$ iff $u^{-1}g' \in \text{nbhd}(u^{-1}g)$).

E.1. Counting shapes in 2D point clouds

Each training / test example consists of up to two instances of each of the following shapes: triangles, squares, pentagons and the "L" shape.

We performed an architecture search on the SetTransformer first and then set the architecture of the LieTransformer such that the models have a similar number of parameters (547k for the SetTransformer and 444k for both LieTransformer-T2 and LieTransformer-SE2) and depth.

Model architecture. The architecture used for the SetTransformer (Lee et al., 2019) consists of 4 layers in the encoder, 4 layers in the decoder and 4 attention heads. No inducing points were used.

The architecture used for both LieTransformer-T2 and LieTransformer-SE2 is made of 4 layers, 8 heads, feature dimension $d_v = 128$ and kernel dim=12. One lift sample was used for each point.

Training procedure. We use Adam (Kingma & Ba, 2014) with parameters $\beta_1 = 0.5$ and $\beta_2 = 0.9$ and a learning rate of $1e-4$. Models are trained with mini-batches of size 32 until convergence.

E.2. QM9

For the QM9 experiment setup we follow the approach of Anderson et al. (2019) for parameterising the inputs and for the train/validation/test split. The value of the f_i are learnable embeddings of each atom type. We split the available data as follows: 100k samples for training, 10% for a test set and the rest used for validation.

We performed architecture and hyperparameter optimisation on the ϵ_{HOMO} task and then trained with the resulting hyperparameters on the other 11 tasks. The model used has 13 layers of attention blocks, using 8 heads (M) in each layer and feature dimension $d_v = 848$. The attention kernel uses the *linear - concat - linear* feature embedding, identity embedding of the Lie algebra elements, and an MLP to combine these embeddings into the final attention coefficients. The final part of the model used had minor differences to the one in diagram 1. Instead of a global pooling layer followed by a 3 layer MLP, a single linear layer followed by global pooling was used. All models were trained using Adam, with a learning rate of $3e-4$ and a batch size of 75. 4 lifting samples were used for each input point ($|\hat{H}| = 4$), with the radius of the neighbourhood η chosen such that the $|\text{nbhd}_\eta(g)| = 50 \forall g \in G$ and we uniformly sample 25 points from this neighbourhood.

Training these models with $T(3)$ and $SE(3)$ equivariance took approximately 2 and 8 days respectively on a single 1080Ti, roughly in line with training the LieConv model.

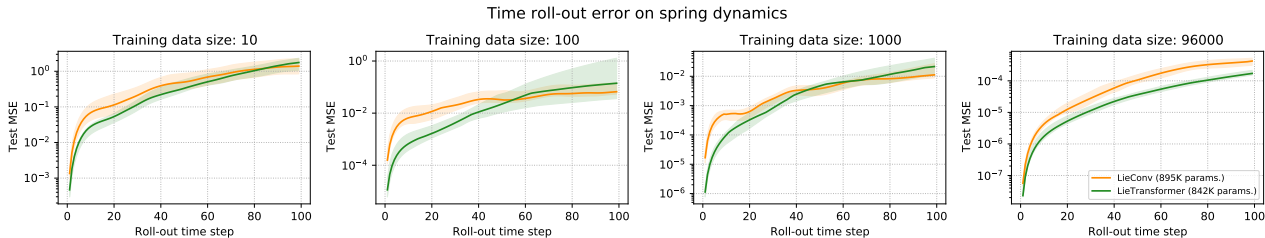


Figure 7. Plots of model error as a function of time step for various data sizes. As can be seen, the LieTransformer generally outperforms LieConv across various training data sizes.

E.3. Hamiltonian dynamics

Spring dynamics simulation. We exactly follow the setup described in Appendix C.4 of Finzi et al. (2020) for generating the trajectories used in the train and test data.

Model architecture. We used a LieTransformer-T2 with 5 layers, 8 heads and feature dimension $d_v = 160$. The attention kernel uses dot-product for the content component, a 3-layer MLP with hidden layer width 16 for the location component and addition to combine the content and location attention components. We use constant normalisation of the weights. We observed a significant drop in performance when, instead of constant normalisation, we used softmax normalisation (which caused small gradients at initialization leading to optimization difficulties). The architecture had 842k parameters. Note that the true Hamiltonian $H(\mathbf{q}, \mathbf{p})$ for the spring system separates as $H(\mathbf{q}, \mathbf{p}) = K(\mathbf{p}) + V(\mathbf{q})$ where K and V are the kinetic and potential energies of the system respectively. Following Finzi et al. (2020), our model parameterises the potential term V .

Training details. To train the LieTransformer, we used Adam with a learning rate of 0.001 with cosine annealing and a batch size of 100. For a training dataset of size n , we trained the model for $400\sqrt{3000/n}$ epochs (although we found model training usually converged with fewer epochs). When $n \leq 100$, we used the full dataset in each batch. For training the LieConv baseline, we used their default architecture and hyperparameter settings for this task, except for the number of epochs which was $400\sqrt{3000/n}$ to match the setting used for training LieTransformer.¹

Loss computation. One small difference between our setup and that of Finzi et al. (2020) is in the way we compute the test loss. Since we compare models’ losses not only over 5-step roll-outs but also longer 100-step roll-outs, we average the individual time step losses using a geometric mean rather than an arithmetic mean as in Finzi et al. (2020). Since the losses for later time steps are typically orders of magnitude higher than for earlier time steps (see e.g. Figure 5), a geometric mean prevents the losses for later time steps from dominating over the losses for the earlier time steps. During training, we use an arithmetic mean across time steps to compute the loss for optimization, exactly as in Finzi et al. (2020). This applies for both LieTransformer and LieConv.

¹This yields better results for the LieConv baseline compared to those reported by Finzi et al. (2020), where they use early stopping and fewer total epochs.

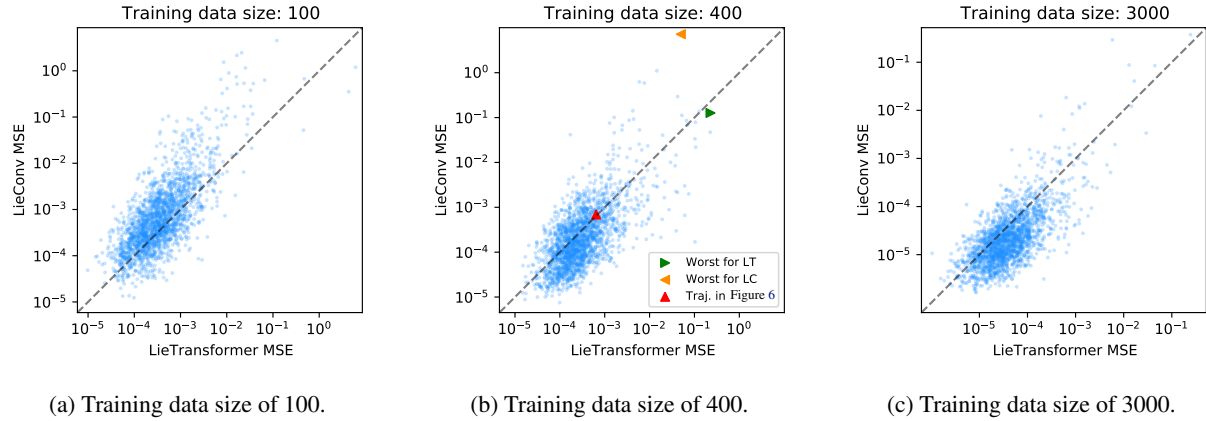


Figure 8. Scatter plots comparing the MSE of the LieTransformer against the MSE of LieConv for various training dataset sizes. Each point in a scatter plot corresponds to a 100-step test trajectory, indicating the losses achieved by both models on that trajectory. In the middle figure we have highlighted the MSEs corresponding to the trajectories shown in Figures 6 and 9.

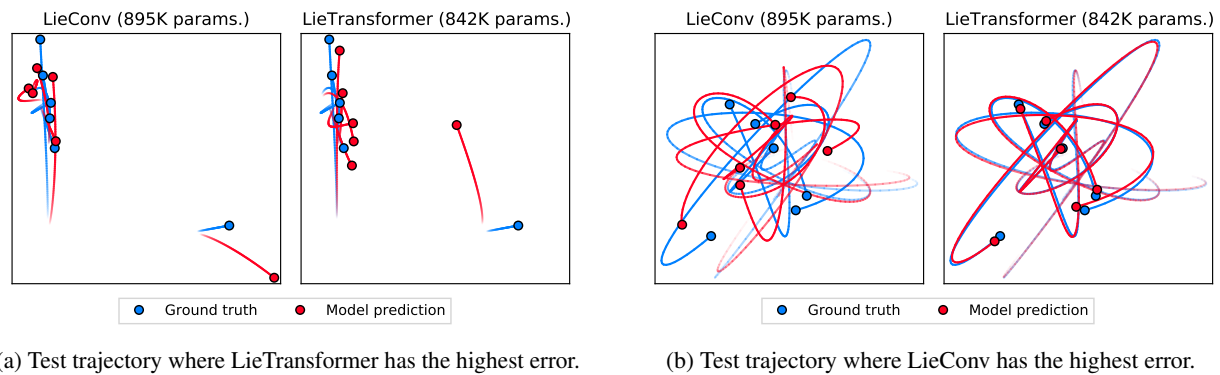


Figure 9. Additional example trajectories comparing LieTransformer and LieConv. Both models are trained on a dataset of size 400. See Figure 8 for a scatter plot showing these test trajectories and the one in Figure 6 in relation to all other trajectories in the test dataset.